Real-Time Visualization and Dynamics of Boron Nitride Nanotubes Undergoing Brownian Motion

Ashleigh D. Smith McWilliams, † Zhao Tang, ‡ Selin Ergülen, † Carlos A. de los Reyes, † Angel A. Martí* † and Matteo Pasquali, † ‡ $^{\xi}$ $^{\xi}$

†Departments of Chemistry, ‡Chemical and Biomolecular Engineering, §Materials Science and Nanoengineering, ¹Bioengineering, and ⁷Smalley-Curl Institute for Nanoscale Science and Technology, Rice University, Houston, Texas 77005, United States.

ABSTRACT. We report the first real-time imaging of individualized BNNTs via stabilization with a Rhodamine surfactant and fluorescence microscopy. We study the rotational and translational diffusion and find them to agree with predictions based on a confined, high aspect-ratio rigid rod undergoing Brownian motion. We find that BNNTs' behavior parallels that of individualized CNTs, indicating that BNNTs could also be used as model semiflexible rods to study soft matter systems, while avoiding CNTs' experimental disadvantages due to their strong light absorption. The use and further development of our technique and findings will accelerate the application of BNNTs, from material engineering to biological studies.

Introduction

Boron nitride nanotubes (BNNTs) are structurally analogous to carbon nanotubes (CNTs) but possess many distinguishing properties that make them ideal candidates for a wide array of

applications. For example, unlike CNTs that are available in metallic or semiconducting forms, BNNTs have a uniform wide band gap of ~ 5.5 eV, making them electrically insulating regardless of chirality or diameter, and nearly transparent to visible light. Additionally, BNNTs have excellent thermal conductivity, on the order of 350 W/mK, which is similar to that of copper.² Finally, they have superb chemical and thermal stability, not undergoing oxidation in air until temperatures greater than 900°C.3 These remarkable properties make BNNTs well suited for a variety of applications, ranging from electronics to material engineering to biomedical applications. 4-12 A fundamental understanding of BNNT dynamics in solution would accelerate research in neat BNNT macroscopic materials, BNNT-polymer composites, and BNNTs in biological systems, as was the case for CNTs. 13-19 In fact, dilute rotational and translational diffusivities are the bases for understanding behavior in crowded systems such as liquid crystals, gels, and polymer networks, and for understanding shear alignment in flow processes, which are key in material processing, biology, composites, and manufacturing, respectively. For example, liquid-phase processing would enable the large-scale production of BNNT films, fibers, and composites.³⁻⁶ Understanding how BNNTs diffuse in solution is paramount to producing aligned films and fibers, as it provides a timescale for relaxation and reorientation. ^{14–16} Additionally, knowing how BNNT diffusion compares to that of other materials, such as polymers, can allow us to design composites that maximize BNNTs' desired properties.^{6,17} Finally, the study of how BNNTs behave in aqueous solution will allow us to more accurately predict their response to environmental changes, such as viscosity or temperature. This is particularly pertinent to biological studies where changes in environment are quite common. 18-20 Moreover, the ability to visualize BNNTs in real time could aid the study of interactions between BNNTs and biomolecules, which is crucial for the application of BNNTs in drug delivery or biological sensors. 9-12 Despite these

important applications, real-time visualization of BNNTs in solution has been extremely limited and the investigation of BNNT dynamics has never been reported.

While ensemble techniques, such as dynamic light scattering and zeta potential, can provide useful information about BNNT dispersions, ^{21–24} the polydispersity of BNNT samples prevents detailed dynamical information from being derived from these results. On the other hand, high resolution imaging techniques, such as atomic force microscopy (AFM) and transmission electron microscopy (TEM), can provide length and diameter information about individual BNNTs, but do not provide real-time dynamics. Fluorescence microscopy allows for real-time dynamics studies at the level of an individual particle or molecule. This technique has been previously utilized to measure diffusion and bending dynamics information for single-walled carbon nanotubes (SWCNTs)^{13,25–28} and germanium nanowires,²⁹ as well as, to perform ground breaking dynamics studies on many biomolecules.^{30–39}

Current progress in real-time visualization of BNNTs is limited due to their poor dispersibility in all solvents and deep-UV excitation and emission (Figure S1). Because imaging in the UV is challenging, fluorescence imaging from direct excitation has not been reported, and an external fluorescent tag must be used. Additionally, since BNNTs are amphiphobic, covalent functionalization or the use of a dispersing agent must be utilized to obtain BNNT dispersions. Political To our knowledge, very little work has been done towards real-time BNNT visualization in solution. Political Recent work in our group has shown that BNNTs can be individualized in solution using cationic surfactants. With this in mind, we synthesized a line of cationic surfactants that have a fluorescent molecule (Rhodamine B) included in the structure and showed that it could be used to individualize and image CNTs and BNNTs. Here, we image BNNTs dispersed in this Rhodamine surfactant and measure their translational and rotational diffusivities in solution,

producing, for the first time, information on the dynamics of these nanostructures, and showing that BNNTs behave as ideal rigid rods.

Experimental Section

Materials. Boron nitride nanotubes were obtained from BNNT, LLC (P2β Type) and purified by a method modified from one previously reported.⁴⁹ Rhodamine B was obtained from Acros and dodecanol was purchased from Sigma-Aldrich. Cetyltrimethylammonium chloride (CTAC) was purchased from TCI America. Glass slides and cover slips were from Thermo Scientific and were sonicated in acetone for 5 minutes, rinsed with isopropanol, and air dried before use.

Synthesis of Rhodamine surfactant. The Rhodamine surfactant with a dodecane group was synthesized by mild esterification reaction based on the Garegg-Samuelsson Reaction,⁵⁰ as previously reported.⁴⁸ A solution of I₂ (38.1 mg, 0.15 mmol) in DCM (~4 mL) was prepared in an oven-dried round-bottom flask equipped with a stir-bar. Ph₃P (39.3 mg, 0.15 mmol), imidazole (22.5 mg, 0.33 mmol), and Rhodamine B (47.9 mg, 0.1 mmol) were added and the solution was stirred at room temperature for 5 minutes. Dodecanol (34 μL, 0.15 mmol) was then added and the solution was left to stir for an additional 24 hours at room temperature, in the dark. The crude product was washed with 2N HCl and water before being dried with Na₂SO₄ and the solvent removed under vacuum. The residue was purified by column chromatography with a solvent system of equal parts acetone, DCM, and hexanes. The product came off as a dark red band and was dried to produce a dark purple solid as the final, pure product (16 mg, 25% yield).

Preparation of microscope sample. A 1 mM solution of the Rhodamine surfactant in methanol was prepared. This was diluted 7x with a 1 wt. % CTAC solution for a final Rhodamine

surfactant concentration of 143 μ M. At this concentration, the 1 wt.% CTAC solution behaves as a Newtonian liquid (Figure S2). 1 mg BNNTs were added to a 15 mL-plastic centrifuge tube with 7 mL of the surfactant mixture and tip ultrasonicated (QSonica Q55, 20 kHz) for 5 seconds, to break apart BNNT bundles without cutting the BNNTs. The resulting suspension was centrifuged at 500g for 30 minutes. The top 80% of the supernatant was removed and the remaining solution and pellet were resuspended in 1 wt. % CTAC. Then, 30 μ L of 10 wt. % silica microspheres (2.01 μ m diameter, Bangs Laboratories) were added to the final suspension. For imaging, 0.6 μ L of the tagged BNNTs and microspheres were drop-casted on a pre-cleaned microscope slide and covered with a coverslip. The sample was then sealed with epoxy to prevent convective flow due to solvent evaporation.

Imaging BNNTs. BNNTs are imaged on a Zeiss Axiovert 200M epi-fluorescence microscope with a TRITC (Rhodamine) filter cube (Chroma; λ_{ex} 527-552/565 dichroic/ λ_{em} 577-632 nm), a 100x oil immersion objective (N.A.=1.3; diffraction limit (d) \approx 200 nm), and a Toupcam industrial digital camera with a 1.4MP Sony CCD sensor (17 frames per second), controlled by ToupView software. Videos are collected for approximately 5 minutes (\sim 5,100 frames). The silica microspheres, which have previously been utilized for these purposes, ^{51–53} could be visualized in the microscope and were checked before recording to ensure they were well spaced, ensuring no interference with diffusion measurements, and not moving, ensuring they were truly defining the confinement of the system.

Spectroscopic studies. Absorbance measurements were acquired using a Shimadzu 2450 UV-Visible spectrophotometer. Photoluminescence spectra were measured with a Horiba Nanolog Spectrophotometer. The samples were excited at 514 nm and recorded from 535 to 720 nm. Timeresolved decays were recorded using an Edinburgh Instruments OD470 single-photon counting

spectrometer with a 443.6 nm picosecond pulse diode laser with a high-speed red detector. BNNT-Rhodamine surfactant samples were prepared by mixing 7 mg BNNTs with 6.65 mL of 1 wt. % CTAC and 0.35 mL of 1 mM Rhodamine surfactant (final Rhodamine surfactant concentration of 0.1mM). This mixture was tip ultrasonicated for 30s and dialyzed against DI water for 24 hours to remove free Rhodamine surfactant.

AFM height studies. AFM samples were prepared by depositing samples, prepared as described for fluorescence microscopy imaging, on a freshly cleaved mica surface (primed with MgCl₂) using a drop-casting method, washing off excess surfactant with water, and drying in the oven. AFM measurements were performed with a Bruker Multimode 8 AFM system in tapping mode using ScanAsyst Air silicon cantilevers. AFM images were processed in Gwyddion and the height profiles of 100 randomly selected BNNTs were collected.

Results and Discussion

The Rhodamine surfactant utilized in our studies was prepared by a mild esterification reaction⁵⁰ between Rhodamine B and dodecanol.⁵⁴ The Rhodamine surfactant with a twelve-carbon chain was chosen due to its relatively low critical micelle concentration and relatively high quantum yield, when compared to surfactants with shorter and longer carbon chains, respectively. BNNTs were dispersed in a mixture of this Rhodamine surfactant and cetyltrimethylammonium chloride (CTAC). Interactions between the BNNTs and the Rhodamine surfactant were first probed spectroscopically (Figure 1a-c). The fluorescent surfactant alone shows a bathochromic shift of 6 nm with respect to the Rhodamine dye. After dispersing BNNTs in the Rhodamine surfactant and removing excess surfactant by dialysis, the Rhodamine surfactant absorbance and emission spectra are also red shifted approximately 5 nm (from 559 to 564 nm and 585 to 591 nm,

respectively) (Figure 1a,b). Additionally, the quantum yield of the Rhodamine surfactant is quenched from 0.26 to 0.06 (Figure 1c). By comparison, mixing the Rhodamine surfactant and CTAC in the same ratio, without the addition of BNNTs, will increase its quantum yield.⁵⁴ Therefore, the observed quenching of the photoluminescence can be attributed to interactions between the Rhodamine core and BNNTs, producing additional pathways for nonradiative decay. This red shift in absorbance and fluorescence quenching has been previously reported for Rhodamine B associated with SWCNTs, and was determined to occur by a static quenching mechanism through the formation of a stable ground state complex.⁵⁵ Finally, the fluorescence lifetime of the Rhodamine surfactant was also measured before and after addition of BNNTs. The Rhodamine surfactant alone resulted in a monoexponential decay with a lifetime of 1.81 ns, similar to that of Rhodamine B. However, when mixed with BNNTs, a biexponential decay was produced, which was deconvoluted to give lifetimes of 0.24 ns (49%) and 1.62 ns (51%), apparently due to Rhodamine surfactant interacting with BNNTs and free in solution, respectively (lifetime decays in Figure S3). These results show that the chosen surfactant system is ideal for optimal contrast in our system. The change in Rhodamine fluorescence demonstrates that the surfactant associates relatively strongly to the BNNT, making it an ideal fluorescent label. Additionally, though the quenching of the Rhodamine's fluorescence may reduce the dye's signal, it also reduces its photobleaching,⁵⁶ meaning the signal remains more stable throughout the experiment, allowing for longer periods of data collection.

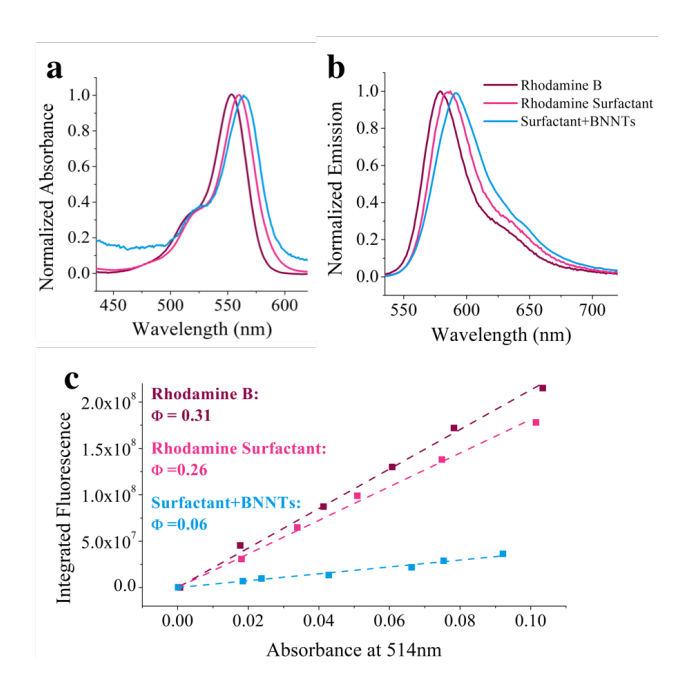


Figure 1. Absorbance spectra (a), photoluminescence spectra (b), and quantum yields (c) for Rhodamine B, Rhodamine surfactant, and Rhodamine surfactant dispersed BNNTs.

Imaging studies were performed using this optimized surfactant system. In order to obtain longer BNNTs, ultrasonication was minimized and the centrifugation pellet was utilized (see Supporting Information). AFM studies of the microscope sample (Figure S4 a-c) show that the suspended BNNTs were primarily individualized (average diameter ~ 7 nm). The sample also contained aggregates and hBN impurities that are easily discerned in the microscope view (Figure S4 d), and, therefore, are easily avoided. The addition of silica microspheres to the solution mixture produced a 2 μ m confinement between the glass slide and coverslip throughout. Confinement in a narrow gap limits the rod diffusion perpendicular to the imaging plane, allowing for longer imaging times where the rod is in focus; moreover, confinement is interesting per-se – in fact, even water behaves differently under confinment, $^{57-59}$ albeit on much smaller length scales. Figure 2 shows time-lapse images of a tagged 3.6 μ m BNNT undergoing Brownian motion (video of BNNT movement available as Supporting Information). We found that using fluorescence microscopy

and the Rhodamine surfactant, BNNTs longer than $\sim 1.5~\mu m$ could be identified and visualized. Each BNNT was imaged for approximately 5 minutes. A control sample containing only the mixture of surfactants was visualized and displayed only a fluorescence background; i.e., no rod-like objects could be found (Figure S5).

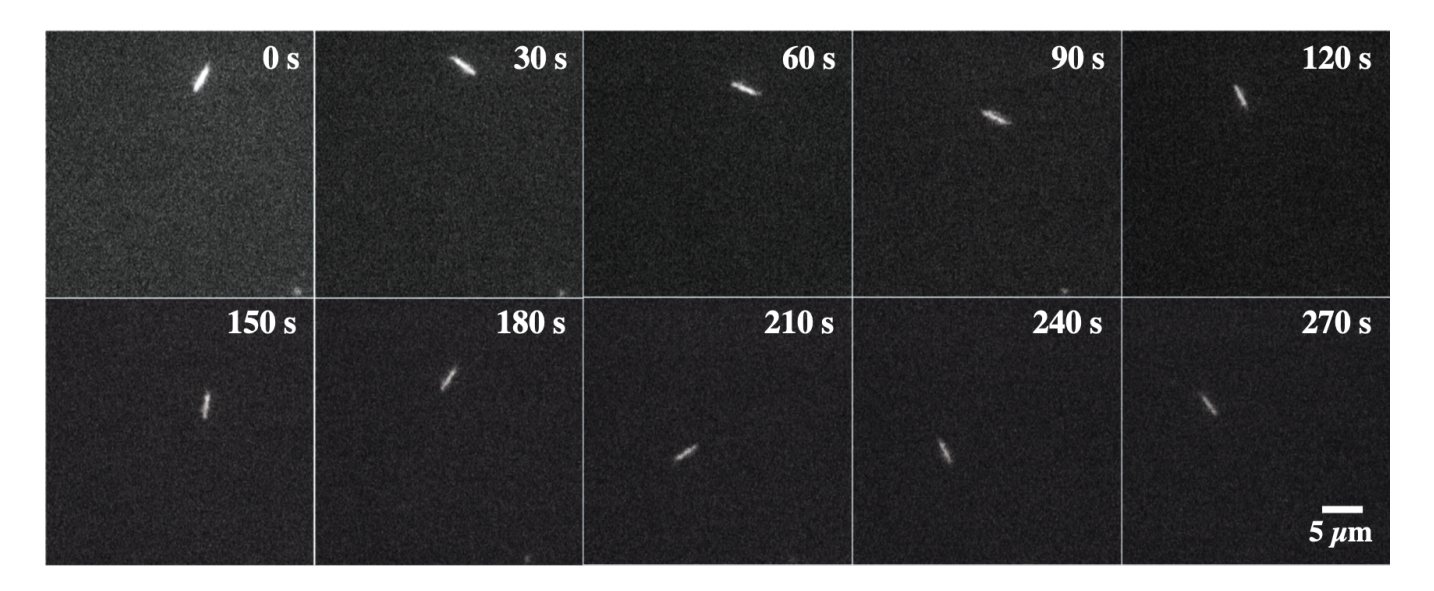


Figure 2. Time-lapse images of a tagged 3.6 μm BNNT undergoing Brownian motion.

The BNNTs remained within the focal plane throughout the 5 minute video; therefore, the center of mass and orientation of the BNNT could be measured for each frame. Figure 3 a-b shows an example of the analyses obtained for a 3.6 μ m BNNT. These data were then used to calculate the mean-squared displacement (MSD) and mean-squared angular displacement (MSAD) of the BNNT (Figure 3 c-d). These displacements were obtained using internal averaging, ⁶⁰ so all position pairs within the same time interval were included for each point. The translational diffusion coefficient (D_t) and rotational diffusion coefficient (D_r) were then calculated. As movement in the z-direction was limited and not measured, the translational diffusion was measured in two dimensions and the rotational diffusion in one dimension. Therefore, MSD =

 $4D_t\Delta t + C$ and MSAD = $2D_r\Delta t + C$, where the constant, C, comes from uncertainty in the measurement, ²⁸ but was found to be negligible in all cases.

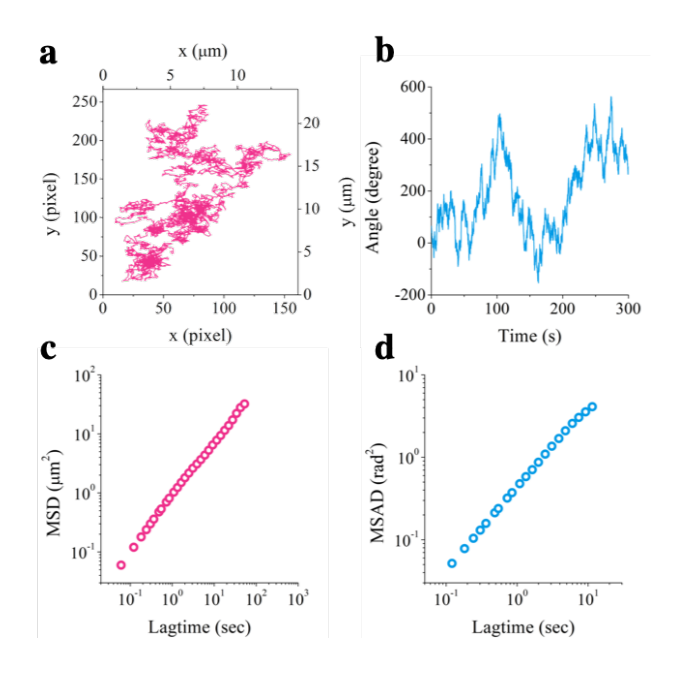


Figure 3. Example analysis of a 3.6 μ m BNNT diffusion. Changes in the center of mass (a), orientation (b), mean squared displacement (c), and mean squared angular displacement (d). Only linear portions of the MSD and MSAD graphs are shown. Linear fits of the MSD and MSAD graphs can then be utilized to calculate the translational (D_t) and rotational (D_r) diffusion coefficients for each BNNT respectively. The slope of the MSD graph equals $4D_t$ and the slope of the MSAD graph equals $2D_r$.

The translational and rotational diffusion coefficients were extracted from trajectories for BNNTs with different lengths, from ~ 1.5 to 4.6 μm . Figure 5 a-b shows the translational and rotational diffusion coefficients plotted as a function of BNNT length. The experimental values were compared to a theoretical rigid rod in bulk solution (dashed line) and under a 2 μm confinement (solid line).³⁶ In bulk fluid, the two-dimensional translational diffusion coefficient and one-dimensional rotational diffusion coefficient for an open cylinder can be given by ⁶¹

$$D_t = \frac{k_B T}{3\pi \eta L} [\ln(p) + X_t(p)] \tag{1}$$

$$D_r = \frac{3k_B T}{\pi \eta L^3} [\ln(p) + X_r(p)]$$
 (2)

where k_B is the Boltzmann constant, T is the temperature, η is the viscosity of the solution (1 mPa s), L is the length of the BNNT, p is the BNNT aspect ratio (length/diameter),

$$X_t(p) = 0.378195 - \frac{1.16052}{\sqrt{p}} + \frac{1.76859}{p} - \frac{0.135408}{p^2} + \frac{0.546373 \ln(p)}{p} - \frac{0.096909 \ln(p)}{p^2}$$

and

$$X_r(p) = -0.492903 - \frac{1.17543}{\sqrt{p}} + \frac{3.16941}{p} - \frac{3.29204}{p^2} + \frac{3.6909}{p^3} - \frac{1.72023}{p^4}$$

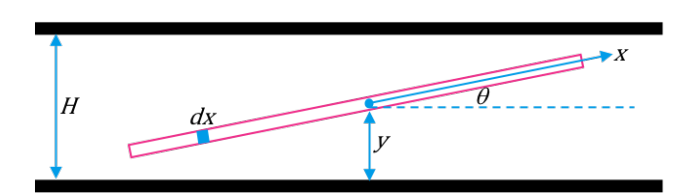


Figure 4. Diagram of a BNNT confined between two glass slides. H is the height between the slide and coverslip, θ is the angle between the BNNT and the slide, and y is the distance between the BNNT center and the bottom glass. The x-axis is along the BNNT axis from the center of the BNNT.

When a rod-like particle is placed under confinement, it experiences additional drag due to interaction with the confining wall (Figure 4).³⁶ This drag depends on the position of the rod between the two slides. An effective drag coefficient can be calculated by averaging over all

allowed states (y and θ). Using the confinement model of Li and Tang,³⁶ the adjusted translational and rotational diffusion coefficients are

$$D_{t} = \frac{\int_{0}^{H/2} dy \int_{-\sin^{-1}(2y/L)}^{\sin^{-1}(2y/L)} D_{t}(y,\theta) d\theta}{\int_{0}^{H/2} dy \int_{-\sin^{-1}(2y/L)}^{\sin^{-1}(2y/L)} d\theta}$$
(5)

where

$$D_t(y,\theta) = \left(\frac{k_B T}{\xi_{\parallel}(y,\theta)} \cos^2\theta + \frac{k_B T}{\xi_{\perp}(y,\theta)} (1 + \sin^2\theta)\right)/2$$

and

$$\xi_{\parallel}(y,\theta) = \int_{-L/2}^{L/2} \left(\frac{2\pi\eta}{\cosh^{-1}[y + x\sin\theta/r]} + \frac{2\pi\eta}{\cosh^{-1}[H - y - x\sin\theta/r]} \right) dx$$

and

$$\xi_{\perp}(y,\theta) = 2\xi_{\parallel}(y,\theta)$$

$$D_r = \frac{\int_0^{H/2} dy \int_{-\sin^{-1}(2y/L)}^{\sin^{-1}(2y/L)} D_r(y,\theta) d\theta}{\int_0^{H/2} dy \int_{-\sin^{-1}(2y/L)}^{\sin^{-1}(2y/L)} d\theta}$$
(6)

where

$$D_r(y,\theta) = \frac{k_B T}{\xi_r(y,\theta)}$$

and

$$\xi_r(y,\theta) = \int_{-L/2}^{L/2} \left(\frac{4\pi\eta \ x^2 \cos^2\theta}{\cosh^{-1}[y + x\sin\theta/r]} + \frac{4\pi\eta \ x^2 \cos^2\theta}{\cosh^{-1}[H - y - x\sin\theta/r]} \right) dx$$

Besides drag, one may expect additional variables, due to coupling of the rotational and translational diffusion, to impact the rod's diffusion when in the presence of a bounding wall. In

fact, recent simulations have shown additional coupling of rod translational and rotational diffusion when rods are very close to a wall (within tens of rod diameters).⁶² This situation can be particularly important for high-density rods (e.g., gold), which tend to concentrate near the bottom of a slit gap. In our experimental setting, gravity has a smaller effect, due to a relatively small density difference between BNNT/surfactant micelles and water (see Supporting Information); therefore, BNNTs are predominantly located near the middle of the gap – where they can access more configurations and hence have higher entropy. Combined with the scattering in the data, this may explain why the experimentally determined rotational and translational diffusions for BNNTs agree well with the simple hydrodynamic confinement model predictions (Figure 5). Additionally, the experimental results show a similar trend to those seen for other rod-like particles, including SWCNTs, actin filaments, and germanium nanowires.^{13,29,36}

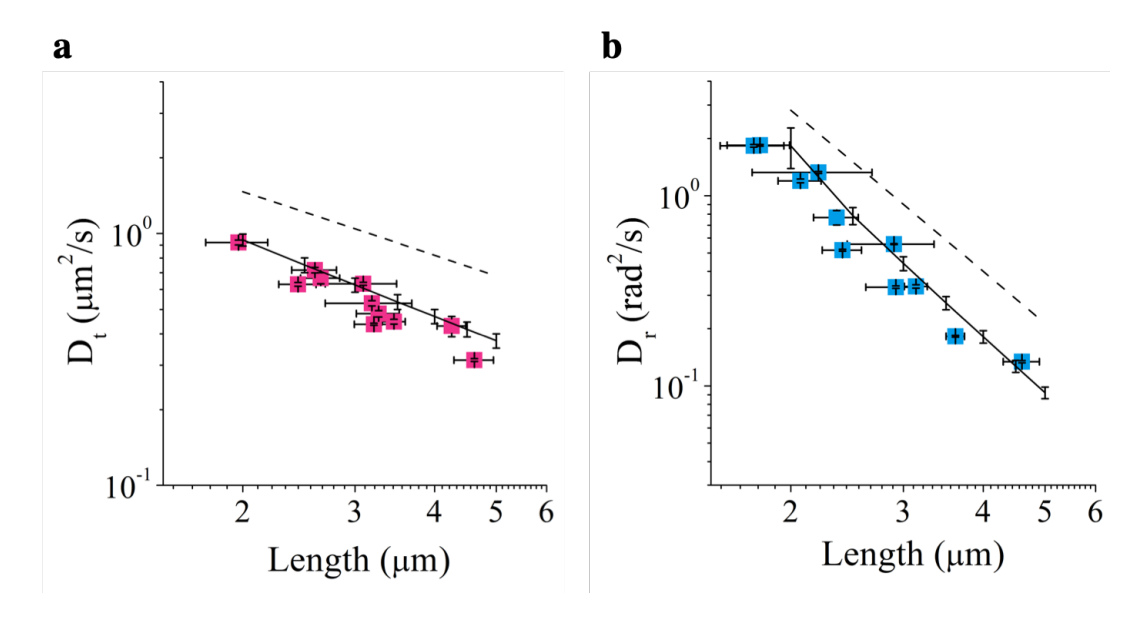


Figure 5. Translational (a) and rotational (b) diffusion coefficients of BNNTs plotted as a function of length and compared to a theoretical rigid rod under a 2 μm confinement according to confinement theory.³⁶ Colored squares represent the experimental measurements, the solid black line represents the confinement theory predicted values, and the dashed line represents predicted

diffusion in bulk fluid.⁶¹ Error bars come from the standard deviation in length measurements and error in the linear fit of the MSD and MSAD data.

The videos of BNNT movement were also analyzed to investigate their bending dynamics. The flexibility of a rod-like particle can be characterized by its bending stiffness and persistence length. According to a continuum model for a hollow cylinder of radius, d, the bending stiffness, $\kappa = \pi C d^3$, where C is the in-plane stiffness. Scaling bending stiffness with thermal energy gives the persistence length, $L_P = \kappa/k_B$. Fakhri *et al.* measured the persistence lengths of SWCNTs, based on the observed bending modes of the SWCNTs, and compared them to those predicted by theory. They found the persistence lengths to range from 26 to 138 μ m; scaling with the cube of the SWCNT diameter, as predicted, but roughly 2x larger than predicted using *ab initio* calculations to determine the SWCNT in-plane stiffness ($C = 345 \text{ J/m}^2$). $C = 345 \text{ J/m}^2$

When analyzing the BNNT videos, no bending modes could be observed, due to diffraction limitations (Figure S6). However, we can calculate the theoretical persistence length using *ab initio* calculations for the in-plane stiffness ($C = 271 \text{ J/m}^2$)⁶³ and AFM measurements for the average diameter (d = 7 nm) (Figure S4 c). This gives a persistence length of ~ 7 mm (around 100x higher than the SWCNT range). This is reasonable because thicker, multiwalled BNNTs (~ 3 concentric layers) are expected to be stiffer than SWCNTs. Considering this approximation, direct imaging of thermal undulations may be possible for BNNTs ~ 70 μ m (Figure S6) or for BNNTs with fewer walls.

Conclusion

In summary, BNNT diffusion in aqueous solution has been investigated for the first time.

We used a fluorescent surfactant that stabilized the BNNT dispersion while also fluorescently

tagging the BNNTs. Spectroscopic measurements show evidence of association between the Rhodamine surfactant and BNNTs, providing better imaging contrast. Videos of BNNT motion yielded translational and rotational diffusion coefficients; these were compared to predicted values for a confined Brownian rigid rod. Both rotational and translational diffusion coefficients agreed with the theoretical values and previous studies on other rod-like particles. ^{13,29,36} The bending dynamics of BNNTs were also analyzed, however, as anticipated by theory (which predicts a persistence length of ~7 mm), BNNT bending mode amplitudes were too small to be detected in our imaging system.

The conclusion that BNNTs undergoing Brownian motion behave like rigid rods is not trivial due to the unique electron density distribution on the surface of BNNTs. Nonetheless, the close correlation between BNNTs and rigid rods implies that aspect ratio and stiffness, which has been well documented for BNNTs, 63,64 are the main factors that modulate the dynamics of BNNTs in solution. Knowing that BNNTs behave as model rigid rods has important repercussions on future development of macroscopic materials using BNNTs as building blocks. First, having a time scale for BNNT relaxation ($\tau = 1/6D_{\tau}$)¹⁵ will be pertinent to the production of aligned BNNT macromaterials, particularly when using flow assembly. Additionally, knowing that BNNTs diffuse similarly to many rigid polymers and other nanomaterials can aid our design and manufacturing of composites that can translate to the macroscale the BNNTs' nanoscale properties. Moreover, since the experimental results for BNNTs fit the theoretical model so well, we can use established theories for crowded rods to predict how the BNNTs' environment, e.g., confinement size, affects their diffusion. This will be particularly useful for biomedical studies, where confinement in the cytoskeleton can dramatically change the dynamics of rods.²⁰

Compared to CNTs, BNNTs have an advantage for studying soft matter systems. Since they behave as rods, like CNTs, they should make liquid crystalline solutions at high concentration. Moreover, because BNNTs are nearly transparent to visible light, such liquid crystalline solutions could be studied using standard optical methods. CNT systems are known to form liquid crystals with complex morphologies and behave unusually at high aspect ratios, forming nematic phases at concentrations as low as 100 ppm;⁶⁵ however, due to their strong light absorption, most studies with CNTs have been limited to thin gaps (below 100 μm and sometimes below 10 μm, where wall interactions dominate domain dynamics)^{66,67} and relatively low concentrations (below 1%). Likewise, metallic nanorods are opaque to light at high concentrations and large gap sizes. ⁶⁸ BNNT liquid crystals would be readily accessible at larger gaps and higher concentrations, and this would allow the exploration of new regimes in liquid crystalline rods. Moreover, the liquid crystalline state is ideal for making aligned macromaterials of nanorods, such as films and fibers, ^{69,70} therefore, studying the phase behavior and dynamics of BNNTs will lead to improved assembly methods for BNNT macromaterials and will also increase our understanding and control of related systems of high technical significance, like CNTs.

ASSOCIATED CONTENT

Supporting Information.

Absorbance and emission profiles of BNNTs in water; lifetime decays of rhodamine B, rhodamine surfactant, and the surfactant-BNNT mixture; AFM analysis of the microscope samples; fluorescence images of aggregates and impurities in a microscope sample; image of surfactant without addition of BNNTs; experimental results of bending stiffness studies; calculation of BNNT-micelle density

The following files are available free of charge via the Internet at http://pubs.acs.org.

Supporting information (PDF)

Video of 3.6µm BNNT undergoing Brownian motion (AVI)

AUTHOR INFORMATION

Corresponding Author

Prof. Matteo Pasquali: mp@rice.edu

Prof. Angel A. Martí: amarti@rice.edu

Author Contributions

The manuscript was written through contributions of all authors. All authors have given approval to the final version of the manuscript.

ACKNOWLEDGMENT

We acknowledge the NSF (CHE 1610175 and 1807737), AFOSR (FA9550-18-1-0014), and the Welch Foundation (C-1668) for their financial support. We thank Thomas Dushatinski (BNNT, LLC) for helpful discussions and assistance procuring material for study.

REFERENCES

- (1) X. Blase, A. Rubio, S.G. Louie, M. L. C. Stability and Band Gap Constancy of Boron Nitride Nanotubes. *Europhys. Lett.* **1994**, *28* (5), 335.
- (2) Chang, C. W.; Fennimore, A. M.; Afanasiev, A.; Okawa, D.; Ikuno, T.; Garcia, H.; Li, D.; Majumdar, A.; Zettl, A. Isotope Effect on the Thermal Conductivity of Boron Nitride Nanotubes. *Phys. Rev. Lett.* **2006**, *97* (8), 085901.
- (3) Lee, C. H.; Bhandari, S.; Tiwari, B.; Yapici, N.; Zhang, D.; Yap, Y. K. Boron Nitride Nanotubes: Recent Advances in Their Synthesis, Functionalization, and Applications. *Molecules* **2016**, *21* (7), 922.
- (4) Zhi, C.; Bando, Y.; Tang, C.; Kuwahara, H.; Golberg, D. Large-Scale Fabrication of Boron Nitride Nanosheets and Their Utilization in Polymeric Composites with Improved Thermal and Mechanical Properties. *Adv. Mater.* **2009**, *21* (28), 2889–2893.

- (5) Li, L.; Li, L. H.; Ramakrishnan, S.; Dai, X. J.; Nicholas, K.; Chen, Y.; Chen, Z.; Liu, X. Controlling Wettability of Boron Nitride Nanotube Films and Improved Cell Proliferation. *J Phys Chem C* **2012**, *116*, 22.
- (6) Terao, T.; Zhi, C.; Bando, Y.; Mitome, M.; Tang, C.; Golberg, D. Alignment of Boron Nitride Nanotubes in Polymeric Composite Films for Thermal Conductivity Improvement. *J Phys Chem C* **2010**, *114*, 4340–4344.
- (7) Del Turco, S.; Ciofani, G.; Cappello, V.; Gemmi, M.; Cervelli, T.; Saponaro, C.; Nitti, S.; Mazzolai, B.; Basta, G.; Mattoli, V. Cytocompatibility Evaluation of Glycol-Chitosan Coated Boron Nitride Nanotubes in Human Endothelial Cells. *Colloids Surf. B Biointerfaces* **2013**, *111*, 142–149.
- (8) Li, Y.; Dorozhkin, P. S.; Bando, Y.; Golberg, D. Controllable Modification of SiC Nanowires Encapsulated in BN Nanotubes. *Adv. Mater.* **2005**, *17* (5), 545–549.
- (9) Ciofani, G.; Vittoria, A. E.; Ae, R.; Ae, A. M.; Cuschieri, A. Folate Functionalized Boron Nitride Nanotubes and Their Selective Uptake by Glioblastoma Multiforme Cells: Implications for Their Use as Boron Carriers in Clinical Boron Neutron Capture Therapy. *Nanoscale Res Lett* **2009**, *4*, 113–121.
- (10) Niskanen, J.; Zhang, I.; Xue, Y.; Golberg, D.; Maysinger, D.; Winnik, F. M. Boron Nitride Nanotubes as Vehicles for Intracellular Delivery of Fluorescent Drugs and Probes. *Nanomedicine Lond* **2016**, *11* (5), 447–463.
- (11) Li, X.; Hanagata, N.; Wang, X.; Yamaguchi, M.; Yi, W.; Bando, Y.; Golberg, D. Multimodal Luminescent-Magnetic Boron Nitride Nanotubes@NaGdF 4:Eu Structures for Cancer Therapy †. *Chem Commun* **2014**, *50*, 4371.
- (12) Chen, X.; Wu, P.; Rousseas, M.; Okawa, D.; Gartner, Z.; Zettl, A.; Bertozzi, C. R. Boron Nitride Nanotubes Are Noncytotoxic and Can Be Functionalized for Interaction with Proteins and Cells. *J. Am. Chem. Soc.* **2009**, *131* (3), 890–891.
- (13) Duggal, R.; Pasquali, M. Dynamics of Individual Single-Walled Carbon Nanotubes in Water by Real-Time Visualization. *Phys. Rev. Lett.* **2006**, *96* (24), 246104.
- (14) Dan, B.; Ma, A. W. K.; Hároz, E. H.; Kono, J.; Pasquali, M. Nematic-Like Alignment in SWNT Thin Films from Aqueous Colloidal Suspensions. *Ind. Eng. Chem. Res.* **2012**, *51* (30), 10232–10237.
- (15) Ma, A. W. K.; Nam, J.; Behabtu, N.; Mirri, F.; Young, C. C.; Dan, B.; Tsentalovich, D.; Majumder, M.; Song, L.; Cohen, Y.; et al. Scalable Formation of Carbon Nanotube Films Containing Highly Aligned Whiskerlike Crystallites. *Ind. Eng. Chem. Res.* **2013**, *52* (26), 8705–8713.
- (16) Hussein, Z.; Rawson, F. J.; Oppenheimer, P. G.; Acton, A.; Mendes, P. M. Length-Selective Chemical Assembly of Vertically Aligned Carbon Nanotubes. *Adv. Mater. Interfaces* **2016**, 3 (11), 1500860.
- (17) Mechrez, G.; Suckeveriene, R. Y.; Zelikman, E.; Rosen, J.; Ariel-Sternberg, N.; Cohen, R.; Narkis, M.; Segal, E. Highly-Tunable Polymer/Carbon Nanotubes Systems: Preserving Dispersion Architecture in Solid Composites via Rapid Microfiltration. *ACS Macro Lett.* **2012**, *I* (7), 848–852.
- (18) Shen, J.-W.; Tang, T.; Wei, X.-H.; Zheng, W.; Sun, T.-Y.; Zhang, Z.; Liang, L.; Wang, Q. On the Loading Mechanism of SsDNA into Carbon Nanotubes. *RSC Adv.* **2015**, *5* (70), 56896–56903.
- (19) Reuel, N. F.; Dupont, A.; Thouvenin, O.; Lamb, D. C.; Strano, M. S. Three-Dimensional Tracking of Carbon Nanotubes within Living Cells. *ACS Nano* **2012**, *6* (6), 5420–5428.

- (20) Fakhri, N.; MacKintosh, F. C.; Lounis, B.; Cognet, L.; Pasquali, M. Brownian Motion of Stiff Filaments in a Crowded Environment. *Science* **2010**, *330* (6012), 1804–1807.
- (21) Yang, M.; Li, M.; Luo, S.; Liang, R. Real-Time Monitoring of Carbon Nanotube Dispersion Using Dynamic Light Scattering and UV-Vis Spectroscopy. *Int. J. Adv. Manuf. Technol.* **2016**, 82 (1–4), 361–367.
- (22) Lee, J.; Kim, J.; Hyeok An, K.; Lee, K.; Young Kim, D.; Jae Bae, D.; Lee, Y. Electrophoretic and Dynamic Light Scattering in Evaluating Dispersion and Size Distribution of Single-Walled Carbon Nanotubes. *J. Nanosci. Nanotechnol.* **2005**, *5*, 1045–1049.
- (23) Sun, Z.; Nicolosi, V.; Rickard, D.; Bergin, S. D.; Aherne, D.; Coleman, J. N. Quantitative Evaluation of Surfactant-Stabilized Single-Walled Carbon Nanotubes: Dispersion Quality and Its Correlation with Zeta Potential. *J. Phys. Chem. C* **2008**, *112* (29), 10692–10699.
- (24) White, B.; Banerjee, S.; O'Brien, S.; Turro, N. J.; Herman, I. P. Zeta-Potential Measurements of Surfactant-Wrapped Individual Single-Walled Carbon Nanotubes. *J. Phys. Chem. C* **2007**, *111* (37), 13684–13690.
- (25) Dmitri A. Tsyboulski; Sergei M. Bachilo, A.; Weisman, R. B. Versatile Visualization of Individual Single-Walled Carbon Nanotubes with Near-Infrared Fluorescence Microscopy. *Nano Lett.* **2005**, *5* (5), 975–979.
- (26) Tsyboulski, D. A.; Bachilo, S. M.; Kolomeisky, A. B.; Weisman, R. B. Translational and Rotational Dynamics of Individual Single-Walled Carbon Nanotubes in Aqueous Suspension. *ACS Nano* **2008**, *2* (9), 1770–1776.
- (27) Fakhri, N.; Tsyboulski, D. A.; Cognet, L.; Weisman, R. B.; Pasquali, M. Diameter-Dependent Bending Dynamics of Single-Walled Carbon Nanotubes in Liquids. *Proc. Natl. Acad. Sci.* **2009**, *106* (34), 14219–14223.
- (28) Streit, J. K.; Bachilo, S. M.; Naumov, A. V.; Khripin, C.; Zheng, M.; Weisman, R. B. Measuring Single-Walled Carbon Nanotube Length Distributions from Diffusional Trajectories. *ACS Nano* **2012**, *6* (9), 8424–8431.
- (29) Marshall, B. D.; Davis, V. A.; Lee, D. C.; Korgel, B. A. Rotational and Translational Diffusivities of Germanium Nanowires. *Rheol. Acta* **2009**, *48*, 589–596.
- (30) Morikawa, K.; Yanagida, M. Visualization of Individual DNA Molecules in Solution by Light Microscopy: DAPI Staining Method. *J. Biochem. (Tokyo)* **1981**, *89* (2), 693–696.
- (31) Yanagida, M.; Hiraoka, Y.; Katsura, I. Dynamic Behaviors of DNA Molecules in Solution Studied by Fluorescence Microscopy. *Cold Spring Harb. Symp. Quant. Biol.* **1983**, *47 Pt 1*, 177–187.
- (32) Houseal, T. W.; Bustamante, C.; Stump, R. F.; Maestre, M. F. Real-Time Imaging of Single DNA Molecules with Fluorescence Microscopy. *Biophys. J.* **1989**, *56* (3), 507–516.
- (33) Smith, S.; Finzi, L.; Bustamante, C.; Chu, S. Direct Mechanical Measurements of the Elasticity of Single DNA Molecules by Using Magnetic Beads. *Science* **1992**, *258* (5085), 1122–1126.
- (34) Duggal, R.; Pasquali, M. Visualization of Individual DNA Molecules in a Small-Scale Coating Flow. *J. Rheol.* **2004**, *48* (4), 745–764.
- (35) Gittes, F.; Mickey, B.; Nettleton, J.; Howard, J. Flexural Rigidity of Microtubules and Actin Filaments Measured from Thermal Fluctuations in Shape. *J. Cell Biol.* **1993**, *120* (4), 923–934.
- (36) Li, G.; Tang, J. X. Diffusion of Actin Filaments within a Thin Layer between Two Walls. *Phys. Rev. E* **2004**, *69* (6), 061921.

- (37) Perkins, T.; Quake; Smith, D.; Chu, S. Relaxation of a Single DNA Molecule Observed by Optical Microscopy. *Science* **1994**, *264* (5160), 822–826.
- (38) Perkins, T. T.; Smith, D. E.; Chu, S. Direct Observation of Tube-like Motion of a Single Polymer Chain. *Science* **1994**, *264* (5160), 819–822.
- (39) Käs, J.; Strey, H.; Sackmann, E. Direct Imaging of Reptation for Semiflexible Actin Filaments. *Nature* **1994**, *368* (6468), 226–229.
- (40) Ciofani, G.; Genchi, G. G.; Liakos, I.; Athanassiou, A.; Dinucci, D.; Chiellini, F.; Mattoli, V. A Simple Approach to Covalent Functionalization of Boron Nitride Nanotubes. *J. Colloid Interface Sci.* **2012**, *374* (1), 308–314.
- (41) Gao, Z.; Zhi, C.; Bando, Y.; Golberg, D.; Serizawa, T. Noncovalent Functionalization of Disentangled Boron Nitride Nanotubes with Flavin Mononucleotides for Strong and Stable Visible-Light Emission in Aqueous Solution. *ACS Appl Mater Interfaces* **2011**, *3*, 20.
- (42) Smith McWilliams, A. D.; de los Reyes, C. A.; Liberman, L.; Ergülen, S.; Talmon, Y.; Pasquali, M.; Martí, A. A. Surfactant-Assisted Individualization and Dispersion of Boron Nitride Nanotubes. *Nanoscale Adv.* **2019**, *I* (3), 1096–1103.
- (43) de los Reyes, C. A.; Walz Mitra, K. L.; Smith, A. D.; Yazdi, S.; Loredo, A.; Frankovsky, F. J.; Ringe, E.; Pasquali, M.; Martí, A. A. Chemical Decoration of Boron Nitride Nanotubes Using the Billups-Birch Reaction: Toward Enhanced Thermostable Reinforced Polymer and Ceramic Nanocomposites. *ACS Appl. Nano Mater.* **2018**, *1* (5), 2421–2429.
- (44) Yu, J.; Chen, Y.; Cheng, B.-M. Dispersion of Boron Nitride Nanotubes in Aqueous Solution with the Help of Ionic Surfactants. *Solid State Commun.* **2009**, *149*, 763–766.
- (45) Gao, Z.; Zhi, C.; Bando, Y.; Golberg, D.; Serizawa, T. Isolation of Individual Boron Nitride Nanotubes via Peptide Wrapping. *J. Am. Chem. Soc.* **2010**, *132* (14), 4976–4977.
- (46) de los Reyes, C. A.; Smith McWilliams, A. D.; Hernández, K.; Walz-Mitra, K. L.; Ergülen, S.; Pasquali, M.; Martí, A. A. Adverse Effect of PTFE Stir Bars on the Covalent Functionalization of Carbon and Boron Nitride Nanotubes Using Billups–Birch Reduction Conditions. *ACS Omega* **2019**, *4* (3), 5098–5106.
- (47) Shin, H.; Guan, J.; Zgierski, M. Z.; Kim, K. S.; Kingston, C. T.; Simard, B. Covalent Functionalization of Boron Nitride Nanotubes via Reduction Chemistry. *ACS Nano* **2015**, *9* (12), 12573–12582.
- (48) Smith McWilliams, A. D.; Ergülen, S.; Ogle, M. M.; de los Reyes, C. A.; Pasquali, M.; Martí, A. A. Fluorescent Surfactants from Common Dyes Rhodamine B and Eosin Y. Pure Appl. Chem. 2020, 92 (2), 265–274.
- (49) Chen, H.; Chen, Y.; Yu, J.; Williams, J. S. Purification of Boron Nitride Nanotubes. *Chem. Phys. Lett.* **2006**, *425* (4–6), 315–319.
- (50) Morcillo, S. P.; Álvarez de Cienfuegos, L.; Mota, A. J.; Justicia, J.; Robles, R. Mild Method for the Selective Esterification of Carboxylic Acids Based on the Garegg–Samuelsson Reaction. *J. Org. Chem.* **2011**, *76* (7), 2277–2281.
- (51) Eichmann, S. L.; Anekal, S. G.; Bevan, M. A. Electrostatically Confined Nanoparticle Interactions and Dynamics. *Langmuir* **2008**, *24* (3), 714–721.
- (52) Eichmann, S. L.; Smith, B.; Meric, G.; Fairbrother, D. H.; Bevan, M. A. Imaging Carbon Nanotube Interactions, Diffusion, and Stability in Nanopores. *ACS Nano* **2011**, *5* (7), 5909–5919.
- (53) Bitter, J. L.; Yang, Y.; Duncan, G.; Fairbrother, H.; Bevan, M. A. Interfacial and Confined Colloidal Rod Diffusion. *Langmuir* **2017**, *33* (36), 9034–9042.

- (54) Smith McWilliams, A. D.; Ergülen, S.; Ogle, M. M.; de los Reyes, C. A.; Pasquali, M.; Martí, A. A. Fluorescent Surfactants from Common Dyes Rhodamine B and Eosin Y. *Pure Appl. Chem.* **2019**.
- (55) Ahmad, A.; Kurkina, T.; Kern, K.; Balasubramanian, K. Applications of the Static Quenching of Rhodamine B by Carbon Nanotubes. *ChemPhysChem* **2009**, *10* (13), 2251–2255.
- (56) Wüstner, D.; Christensen, T.; Solanko, L. M.; Sage, D. Photobleaching Kinetics and Time-Integrated Emission of Fluorescent Probes in Cellular Membranes. *Molecules* **2014**, *19* (8), 11096–11130.
- (57) Giovambattista, N.; Rossky, P. J.; Debenedetti, P. G. Computational Studies of Pressure, Temperature, and Surface Effects on the Structure and Thermodynamics of Confined Water. *Annu. Rev. Phys. Chem.* **2012**, *63* (1), 179–200.
- (58) Giovambattista, N.; Rossky, P. J.; Debenedetti, P. G. Effect of Pressure on the Phase Behavior and Structure of Water Confined between Nanoscale Hydrophobic and Hydrophilic Plates. *Phys. Rev. E* **2006**, *73* (4), 041604.
- (59) Giovambattista, N.; Debenedetti, P. G.; Rossky, P. J. Hydration Behavior under Confinement by Nanoscale Surfaces with Patterned Hydrophobicity and Hydrophilicity. *J. Phys. Chem. C* **2007**, *111* (3), 1323–1332.
- (60) Saxton, M. J. Single-Particle Tracking: The Distribution of Diffusion Coefficients. *Biophys. J.* **1997**, *72*, 1744–1753.
- (61) Aragon, S. R.; Flamik, D. High Precision Transport Properties of Cylinders by the Boundary Element Method. *Macromolecules* **2009**, *42* (16), 6290–6299.
- (62) Yang, Y.; Bevan, M. A. Interfacial Colloidal Rod Dynamics: Coefficients, Simulations, and Analysis. *J. Chem. Phys.* **2017**, *147* (5), 054902.
- (63) Kudin, K. N.; Scuseria, G. E.; Yakobson, B. I. C 2 F, BN, and C Nanoshell Elasticity from Ab Initio Computations. *Phys. Rev. B* **2001**, *64*, 235406.
- (64) Garel, J.; Leven, I.; Zhi, C.; Nagapriya, K. S.; Popovitz-Biro, R.; Golberg, D.; Bando, Y.; Hod, O.; Joselevich, E. Ultrahigh Torsional Stiffness and Strength of Boron Nitride Nanotubes. *Nano Lett.* **2012**, *12* (12), 6347–6352.
- (65) Tsentalovich, D. E.; Ma, A. W. K.; Lee, J. A.; Behabtu, N.; Bengio, E. A.; Choi, A.; Hao, J.; Luo, Y.; Headrick, R. J.; Green, M. J.; et al. Relationship of Extensional Viscosity and Liquid Crystalline Transition to Length Distribution in Carbon Nanotube Solutions. *Macromolecules* **2016**, *49* (2), 681–689.
- (66) Jamali, V.; Behabtu, N.; Senyuk, B.; Lee, J. A.; Smalyukh, I. I.; van der Schoot, P.; Pasquali, M. Experimental Realization of Crossover in Shape and Director Field of Nematic Tactoids. *Phys. Rev. E* 2015, 91 (4), 042507.
- (67) Davis, V. A.; Ericson, L. M.; Parra-Vasquez, A. N. G.; Fan, H.; Wang, Y.; Prieto, V.; Longoria, J. A.; Ramesh, S.; Saini, R. K.; Kittrell, C.; et al. Phase Behavior and Rheology of SWNTs in Superacids. *Macromolecules* **2004**, *37* (1), 154–160.
- (68) Murali, S.; Xu, T.; Marshall, B. D.; Kayatin, M. J.; Pizarro, K.; Radhakrishnan, V. K.; Nepal, D.; Davis, V. A. Lyotropic Liquid Crystalline Self-Assembly in Dispersions of Silver Nanowires and Nanoparticles. *Langmuir* **2010**, *26* (13), 11176–11183.
- (69) Davis, V. A.; Parra-Vasquez, A. N. G.; Green, M. J.; Rai, P. K.; Behabtu, N.; Prieto, V.; Booker, R. D.; Schmidt, J.; Kesselman, E.; Zhou, W.; et al. True Solutions of Single-Walled Carbon Nanotubes for Assembly into Macroscopic Materials. *Nat. Nanotechnol.* 2009, 4 (12), 830–834.

(70) Jiang, C.; Saha, A.; Young, C. C.; Hashim, D. P.; Ramirez, C. E.; Ajayan, P. M.; Pasquali, M.; Martí, A. A. Macroscopic Nanotube Fibers Spun from Single-Walled Carbon Nanotube Polyelectrolytes. *ACS Nano* **2014**, *8* (9), 9107–9112.

TOC Graphic

